Development of magnetorheological elastomers-based tuned mass damper for building protection from seismic events

Shuaishuai Sun
University of Wollongong, ss886@uowmail.edu.au

Jian Yang
University of Science and Technology of China, jy937@uowmail.edu.au

Haiping Du
University of Wollongong, hdu@uow.edu.au

Shiwu Zhang
University of Science and Technology of China, zhangs@uow.edu.au

Tianhong Yan
China EP Equipment Co Ltd, China Jiliang University, thyan@163.com

See next page for additional authors

Recommended Citation

Development of magnetorheological elastomers-based tuned mass damper for building protection from seismic events

Abstract

This study investigated and evaluated a semi-active tuned mass damper which incorporated four multi-layered structures fabricated using magnetorheological elastomers. The four magnetorheological elastomer structures formed a square and provided the tuned mass damper variable stiffness used to track the excitation frequencies. This design not only increases the stability of the tuned mass damper but more importantly eliminates the magnetic circuit gap in a design which we used in the past because all four of the magnetic circuits used to control the magnetorheological elastomer isolators are closed circuits. In order to verify the capability of the magnetorheological elastomer-based tuned mass damper to protect a building from earthquake, extensive simulation and experimental testing were conducted. The swept sinusoidal signal and the scaled 1940 El Centro earthquake record were used to excite a scaled three-story building. Both simulation and experiment have verified that the magnetorheological elastomer-based tuned mass damper outperformed all other passive tuned mass dampers under either swept sinusoidal or seismic conditions.

Disciplines

Engineering | Science and Technology Studies

Publication Details

Authors

Shuaishuai Sun, Jian Yang, Haiping Du, Shiwu Zhang, Tianhong Yan, Masami Nakano, and Weihua Li

Development of magnetorheological elastomers based tuned mass damper for building protection from seismic events

Shuaishuai Sun[1], Jian Yang[1], Haiping Du[2], S.W. Zhang[3], Tianhong Yan[4], Masami Nakano[5], and Weihua Li[1]

Abstract

This study investigated and evaluated a semi-active tuned mass damper which incorporated four multi-layered structures fabricated using magnetorheological elastomers. The four magnetorheological elastomer structures formed a square and provided the tuned mass damper variable stiffness used to track the excitation frequencies. This design not only increases the stability of the tuned mass damper but more importantly eliminates the magnetic circuit gap in a design which we used in the past because all four of the magnetic circuits used to control the magnetorheological elastomer isolators are closed circuits. In order to verify the capability of the magnetorheological elastomer-based tuned mass damper to protect a building from earthquake, extensive simulation and experimental testing were conducted. The swept sinusoidal signal and the scaled 1940 El Centro earthquake record were used to excite a scaled three story building. Both simulation and experiment have verified that the magnetorheological elastomer-based tuned mass damper outperformed all other passive tuned mass dampers under either swept sinusoidal or seismic conditions.

Key Words

Tuned mass damper, Building protection, Magnetorheological elastomers, Vibration control

INTRODUCTION

The passive tuned mass damper (TMD), which consists of a mass, a stiffness element, and a damping component, is undoubtedly a simple, economic, and reliable choice for vibration suppression. These devices protect the primary structure from undesired vibration through the absorption and dissipation of energy by matching their natural frequency to the vibration frequency. In 1928, a classic design of TMD used for an undamped single degree of freedom structure was investigated and optimized (Ormondroyd, 1928, Den Hartog and Ormondroyd, 1928). Since then, TMDs have been extensively studied and employed to a wide variety of structures in the fields of civil and mechanical engineering (Matta, 2011, Schramm et al., 2010, QIN et al., 2009), but the inherent passive nature causes a narrow band of effective frequency, ineffective reduction of frequency changing vibration, and detuning, and these factors limit their effectiveness. (Walsh and Lamancusa, 1992). In order to make the TMDs more adaptive, many controllable TMD designs have been developed (Fisco and Adeli, 2011a, Fisco and Adeli, 2011b). The addition of an active force actuator to the passive TMD proved to be considerably more effective (Chang and Soong, 1980). Even though the active TMD provides a better vibration suppression response than the passive TMD (Spencer Jr and Nagarajaiah, 2003), its high power consumption, high cost and difficulty of maintenance make the active TMD less reliable than the passive TMD.

In order to overcome these drawbacks but still keep the benefits of both the active TMD and the passive TMD, the concept of the semi-active TMD has been introduced. Semi-active TMD means its

[1]School of Mechanical, Materials and Mechatronic Engineering, University of Wollongong, NSW, Australia

[2]School of Electrical, Computer and Telecommunications Engineering, University of Wollongong, NSW, Australia

[3]Department of Precision Machinery and Precision Instrumentation, University of Science and Technology of China, Hefei, Anhui province, China

[4] School of Mechanical and Electrical Engineering, China Jiliang University, Hangzhou, Zhejiang province, China.

[5] Intelligent Fluid Control Systems Laboratory, Institute of Fluid Science, Tohoku University, Sendai, Japan.

stiffness or damping can be controlled to adapt to different excitations. In recent years, its application has been extended from the vehicle vibration control to structural vibration control (Kwok and Samali, 1995, Ricciardelli et al., 2000, Pinkaew and Fujino, 2001, Sun and Nagarajaiah, 2014, Ji et al., 2005, Aldemir, 2003). To achieve a tunable natural frequency, many methods have been developed for semi-active TMDs. For example, shape memory alloys, piezo stacks, and other active elements were used to control the semi-active TMD's natural frequency (Gsell et al., 2007, Nagarajaiah and Sonmez, 2007, Xu et al., 2011) . Semi-active TMD with variable stiffness was also developed using piezo-electrics or controllable friction devices (Jiang and Hanagan, 2006, Lin et al., 2010). Magnetorheological (MR) technology was also used to control the vibration of the main structure (Weber and Maślanka, 2012, Weber et al., 2011, Sun et al., 2014, Sun et al., 2015a). The effectiveness of semi-active TMD with a magnetorheological damper used for the response control of a wind-excited tall building was investigated in (Kang et al., 2011). Analysis has shown that the semi-active TMD can reduce the structural responses in a way which is similar to an active TMD but with a significant reduction in power consumption. Lin (Lin et al., 2005) also proposed a semi-active TMD with an MR damper to illustrate the control effect of the semi-active TMD. The numerical simulation results show that the semi-active TMD has much greater control efficiency than passive TMD. Most of the currently proposed MR-based TMDs use the magnetorheological fluid as the controllable component but this has an inherent disadvantage when it is used to develop semi-active TMD. The reason for this is that the aim of the semi-active TMD is to control its natural frequency to trace excitation frequency variation; however the natural frequency of the TMD is directly determined by its stiffness instead of the damping. This means that, magnetorheological fluid is not an ideal material to establish semi-active TMD, even though it can improve the vibration suppression to a certain extent.

Magnetorheological elastomers (MRE), as a solid counterpart of magnetorheological fluid, can increase their elastic modulus or stiffness monotonically as the magnetic field increases

(Padalka et al., 2010, Han et al., 2013), and then immediately revert to its initial status when the magnetic field is removed. Because of this smart nature, MRE has been used to implement smart devices such as MRE absorbers and MRE isolators (Liao et al, 2016, Behrooz et al, 2014, Fu et al, 2016). For example, Behrooz et al proposed a variable stiffness and damping isolator (VSDI) and used four of it to build and test an integrated system. Experimental results show that the natural frequency of the VSDI is controllable and that the VSDIs can be used as a controllable base isolator.
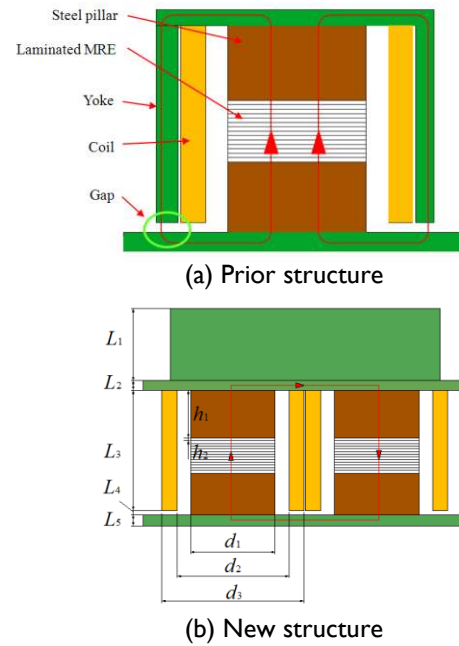

Figure 1. Sketches of the laminated MRE devices

The incorporation of MRE into TMD will also enable the natural frequency of the TMD to be controllable so as to deal with the variations in excitation frequency of different kinds of earthquakes. To the best of our knowledge, the existing literature includes little research into MRE-based semi-active TMD. Some research has been reported in the existing literature regarding the application of single-layered MRE on vibration control but these devices cannot meet the requirements of the TMD such as large lateral strain, high vertical support capability and low natural frequency (Sun et al., 2015b). In this paper, an innovative MRE-based TMD aimed at protecting buildings from earthquakes is developed based on the previously developed multilayered MRE structure (Yang et al., 2014, Yang et al., 2013). The proposed MRE TMD used the multi-layered MRE

and steel structure in order to have greater lateral flexibility and high vertical support capability. Four MRE structures in a square layout make the TMD more stable and able to avoid tilting under serious vibration and, even more importantly, form four totally closed magnetic circuits which decrease the magnetic resistance of the magnetic circuit. Section "The structure and working principle of the innovative MRE TMD" introduces the detailed design of the magnetorheological elastomer tuned mass damper. Section "Frequency Shift range Test of The MRE TMD" examines the frequency shift property. Section "Simulation of the scaled building with MRETMD" describes the simulation. Section "Experimental verification" examines the effectiveness of the MRE TMD and the last section draws the conclusion.
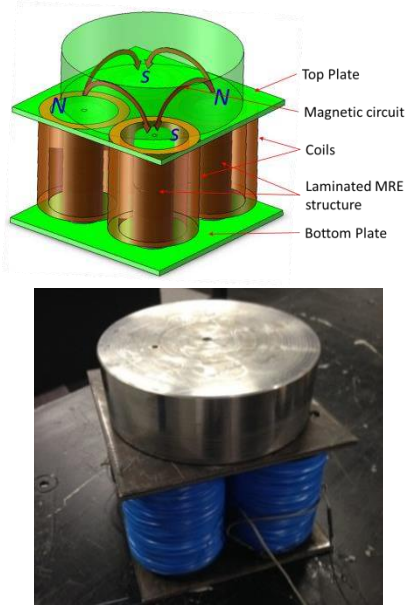

Figure 2. Design and photograph of the MRE TMD

The structure and working principle of the innovative MRE TMD

One of the innovations of the current research is the adoption of four multilayered MREs and steel structures. In our prior research, the multi-layered structure was used for MRE isolators (Yang et al., 2014, Yang et al., 2013) and absorbers (Sun et al., 2015b) because it not only improves the overall conductivity of the MRE but also enables large lateral strains. However, the big challenge is the inevitable gap between the yoke and the bottom plate, as shown in Figure 1 (a) (Li and Li, 2015). This gap increases the magnetoresistance of the

magnetic circuit and hence decreases the variation range of the MRE stiffness. To avoid this, the present study proposes an innovative design which gathers together four multi-layered MRE structures, as shown in Fig.1 (b). It can be seen that the four multi-layered structures form a square layout, and this increases the stability of the MRE TMD while still retaining sufficient lateral flexibility. These four coils are connected in series before current is applied. The most noteworthy point of this design is that one totally closed magnetic circuit forms between any two adjacent multi-layered structures and this means that there is a total of four closed magnetic circuits. Any two adjacent structures have opposed winding directions of their solenoids, so that they will generate opposite magnetic fields when the current is applied. It can be seen from Figure 2 that the magnetic induction lines come out of the N-polar of one solenoid and go inside the S-pole of the adjacent solenoid, or vice versa. The clear advantage of this design is that it eliminates the usage of the gap and guarantees that the overall magnetic resistance of the magnetic circuit reduces.

The prototype of the innovative MRE TMD is shown in Figure 2. Carbonyl iron particles (C3518, Sigma-Aldrich Pty Ltd), silicon rubber (Selleys Pty. Ltd), and silicon oil (Sigma-Aldrich Pty. Ltd) are used to fabricate the MRE layers and their weight ratio is 7:2:1. After mixing them thoroughly in a container, a vacuum case was used to remove the air bubbles inside the mixture. Then the MRE samples were cured in a mould under no magnetic field for 5 days. Then 10 layers of the MRE sheets were bonded with steel sheets layer by layer to produce four laminated MRE-steel pillars. The whole core structure was then fixed to the top plate of the TMD, and then a steel cylinder and solenoid were also fixed to the top plate. The last step was to fix the laminated MRE pillar to the bottom plate. The detailed size of the MRE TMD is shown in table 1.

Table.1. Parameters of MRE TMD

Parameters	Values	Parameters	Values
h_1	40 mm	L_1	50 mm
h_2	1 mm	L_2	5 mm
d_1	35 mm	L_3	100 mm
d_2	55 mm	L_4	5 mm
d_3	80 mm	L_5	5 mm
coil	1000 turns		

After prototype was constructed, the magnetic flux density passing through the MRE was calculated using FEA method available in COMSOL software. As a comparison, we also analyzed the magnetic flux density passing through MRE in our prior structure, as shown in Figure 1(a). The resistance and turns of each coil and the dimension of MRE in the two structures are the same. The relative permeability of MRE was defined based on the B-H relationship provided by Xing et al, 2015, for the same fabricated 7:2:1 weight ratio MRE. Figure 3 and Figure 4 show the flux density analysis for the new structure and the prior structure, respectively. Figure 5 shows the comparison between the two magnetic flux density analyses. The x axis indicates the position from the top of the laminated MRE structure to the bottom. It can be seen that the magnetic flux density generated by the new structure is stronger than that generated by the prior one. This means that the new structure is superior to the prior one in producing stronger magnetic field.
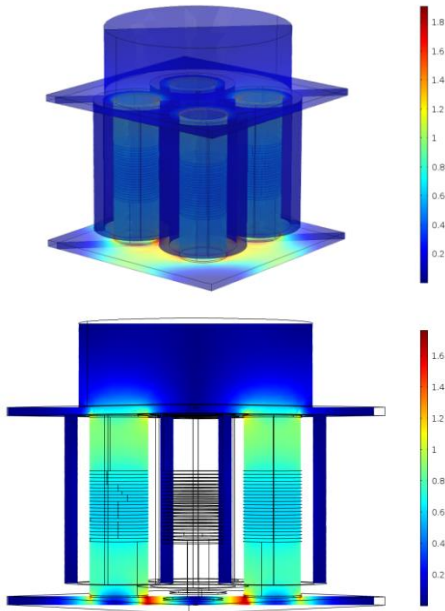

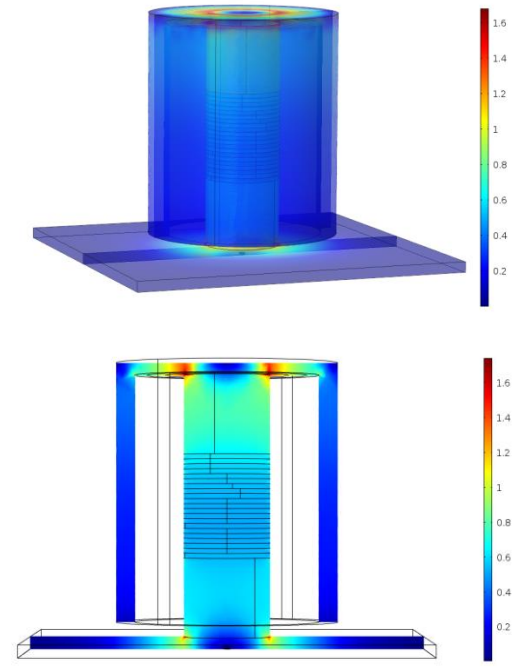Figure 3. Magnetic flux density analysis for the new structure.

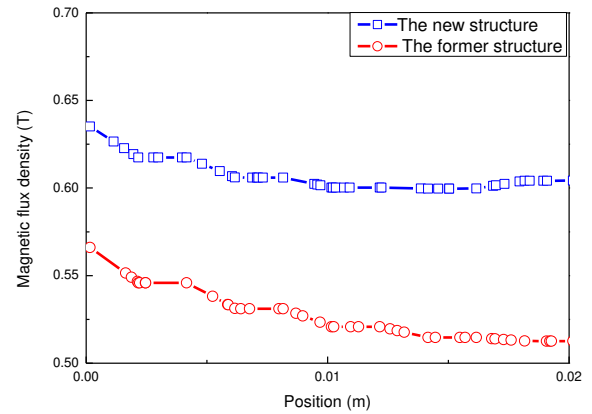Figure 4. Magnetic flux density analysis for the prior structure.

Figure 5. Comparison between the two magnetic flux density

The working principle of this MRE TMD is detailed as follows. The working mechanism of the semi-active TMD is to tune its natural frequency to trace the excitation frequency from the earthquake. In terms of MRE TMD, the magnetic field passing through the MRE can be generated by the coil and controlled by the current from an external DC power source. The shear modulus of the MRE is determined by the strength of the magnetic field, and the shear modulus determines the stiffness of the MRE TMD. As a consequence, the natural frequency of the MRE TMD can be controlled by adjusting the current in the coil so that when the natural frequency of the MRE TMD matches the excitation frequency, the vibration can be suppressed quite significantly. This means that the

MRE TMD can tune its own natural frequency to adapt to different earthquakes.

Frequency Shift range Test of The MRE TMD

Experimental setup

The frequency-shift range means the natural frequency variation range of the MRE TMD under different currents and is a key criterion to evaluate the effectiveness and controllability of a semi-active MRE TMD. In this experiment, a series of tests using swept sinusoidal signals were conducted to measure the frequency-shift performance. Figure 6 illustrates the detailed experimental setup, which consists of the shaker and the horizontal vibration platform. The MRE TMD was fixed onto the platform with two accelerometers (CA-YD-106) installed onto the top and bottom plates, respectively, measuring their lateral accelerations. This vibration platform was forced to vibrate horizontally by a shaker (VTS, VC 100-8) driven by a harmonic signal generated by a computer and amplified by a power amplifier (YE5871). A DC power supply (THURLBY-THANDAR, INSTRUMENTS LTD) was used to provide current signals to the solenoids. A data acquisition board was used as the interface between the hardware and the software and transferred the measured accelerations to the computer. The signal collection, recording, and processing were developed using the LabVIEW program. With this system, the transmissibility of the laminated MRE TMD under different currents was recorded and displayed directly onto the computer.
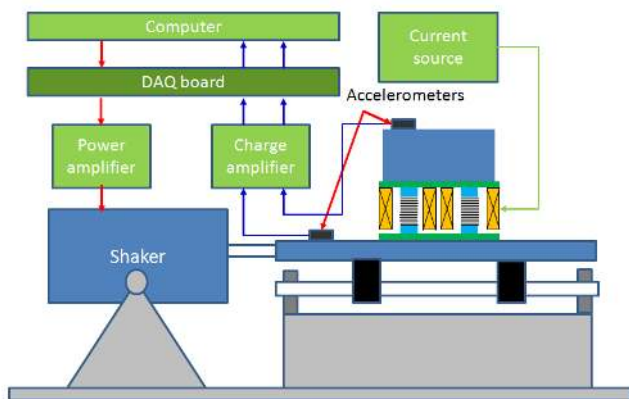

Figure 6. Experimental set-up for testing the frequency shift property of MRE TMD.

Test results

In this test, the DC current varied from 0A to 2.5A in steps of 0.5A. A total of 6 tests were conducted. Figure 7 records the frequency-shift performance (transmissibility and phase) under various current conditions. It can be seen that the natural frequency increased from 3.1Hz to 7.1Hz when the current was changed from 0A to 2.5A.
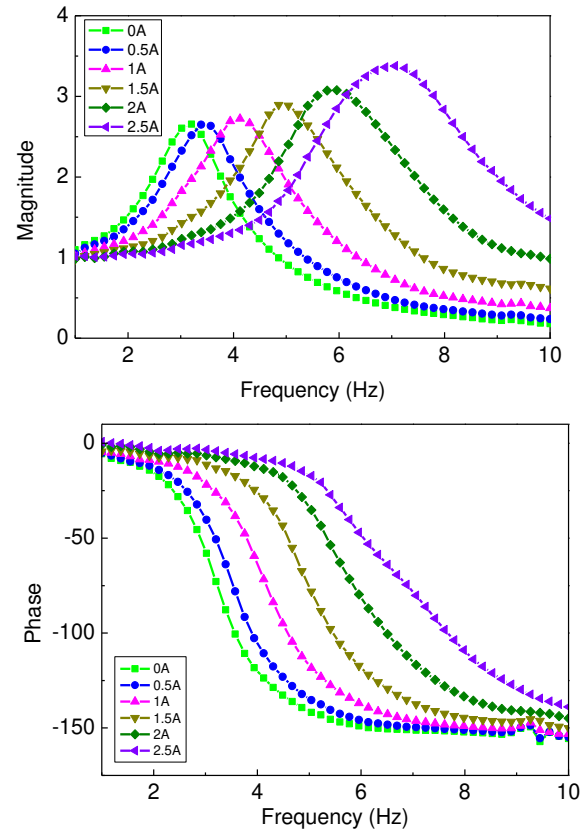

Figure 7. Transmissibility of the MRE TMD under different currents

Simulation of the scaled building with MRE TMD

Modelling of the building with MRE TMD

A three storey building model was designed and built. All the variables and dimensions were scaled down according to the scaling laws in (Mills, 1979). The height of the building is 0.75m, corresponding to the measurements of a real three-storey building of approximately 6.75m in height. By considering a three degrees-of-freedom linear building structure with an MRE TMD on the top subject to ground motion, as shown in Figure 8, the motion equations can be written as:

$$m_2\ddot{x}_2 + c_2(\dot{x}_2 - \dot{x}_3) + k_2(x_2 - x_3) + c_1\dot{x}_2 + k_1x_2 = m_2\ddot{x}_g \tag{1}$$

$$m_3\ddot{x}_3 - c_2(\dot{x}_2 - \dot{x}_3) - k_2(x_2 - x_3) + c_{\text{TMD}}(\dot{x}_3 - \dot{x}_4) + k_{\text{TMD}}(x_3 - x_4) = m_3\ddot{x}_g \tag{2}$$

$$m_{TMD}\ddot{x}_4 - c_{TMD}(\dot{x}_3 - \dot{x}_4) - k_{TMD}(x_3 - x_4) = m_{TMD}\ddot{x}_g \tag{3}$$

where m_i (i=1, 2, 3) is the mass of the ith floor; x_i (i=1, 2, 3) is the relative displacement of the ith floor with respect to the ground; c_i (i=1, 2)=25Ns/m and k_i (i=1, 2)=55032 N/m are the damping and stiffness coefficients of inter-floors, respectively; m_{TMD} = 14.2kg is the mass of the TMD; c_{TMD} and k_{TMD} are the current-dependent damping and stiffness coefficients of the MRE TMD, respectively. The masses of the building model are identical for each storey unit and m_i=25Kg, for i=1, 2, 3. The stiffness and damping of the TMD under different currents, k_{TMD} and c_{TMD}, were tested and are given in Table 2.

Table 2 The values for k_{TMD} and c_{TMD}

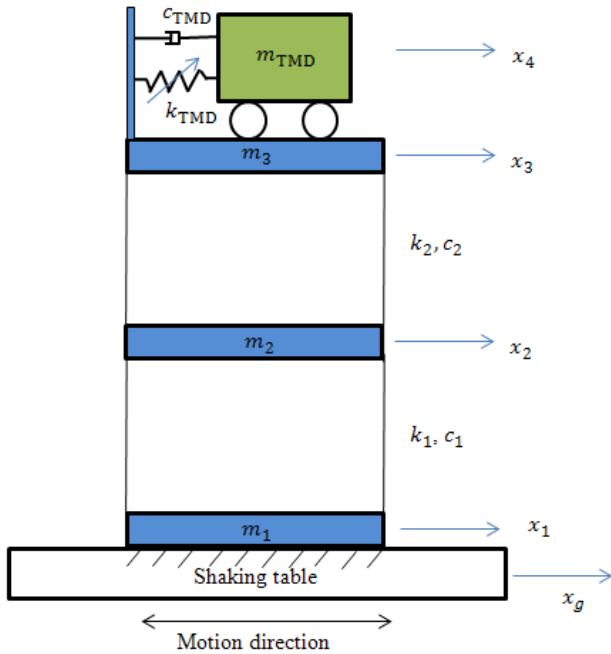| Current	0A	0.5A	1A	1.5A	2A	2.5A
k_{TMD} (N/m)	5823	6358	9663	14056	18228	21945
c_{TMD} (Ns/m)	52	63	74	87	108	121

Figure 8. Mathematical model of the scaled building.

Control algorithms

Corresponding to the two different excitations (sweep frequency excitation and earthquake excitation), two different control algorithms are proposed: short time Fourier transform based frequency tracing control and fuzzy logic control, respectively. In terms of the sweep frequency excitation, the short time Fourier transform control algorithm can calculate the frequency of the excitation and then control the natural frequency of MRE TMD to trace it (Sun et al., 2015b). The short time Fourier transform control algorithm, however, is not the best option for earthquakes because it is a multiple frequency excitation. As a result, fuzzy logic control was used in order to deal with the earthquake excitation.

Short time Fourier transform control algorithm.
The working principle of the short time Fourier transform control algorithm is explained by the following equations.

For the first step, the time segment can be calculated by multiplying the signal $x(t)$ by a window function h(t):

$$x_\tau(t) = x(t)h(t - \tau) \tag{4}$$

where τ is the fixed time, and t is the running time. The hamming window is used as the window function. After that, the Fourier transform for the modified signal is calculated as:

$$X_\tau(\omega) = \frac{1}{\sqrt{2\pi}} \int x(t)h(t-\tau)e^{-j\omega t}dt \tag{5}$$

The energy density of the windowed signal at fixed time τ can be calculated by:

$$P(\tau, \omega) = |X_\tau(\omega)|^2$$
$$= \left|\frac{1}{\sqrt{2\pi}} \int x(t)h(t-\tau)e^{-j\omega t}dt\right|^2 \tag{6}$$

which can provide the time–frequency distribution. Then the instantaneous frequency at time τ is given by:

$$\langle\omega\rangle_\tau = \frac{1}{|x(\tau)|^2} \int \omega |X_\tau(\omega)|^2 d\omega \tag{7}$$

After determining the excitation frequency, the natural frequency of the MRE TMD must be tuned to trace the excitation frequency so that the building's vibration can be attenuated. In other words, the desired natural frequency of the MRE TMD can be known. Based on the relationship between current I and the natural frequency of the MRE TMD given in Figure 7, the desired current can be calculated.

Table 3. The inference rules of the fuzzy logic

Variables	Fuzzy logic rules			
$x_4 - x_3$	N	N	P	P
$\dot{x}_4 - \dot{x}_3$	N	P	P	N
MRETMD stiffness	Hard	Soft	Hard	Soft
Current	L	S	L	S

Fuzzy logic controller
Fuzzy logic control can offer a simple and robust framework for specifying nonlinear control laws that can deal with uncertainty and imprecision

(Subramaniam et al., 1996, Zhou et al., 2002). Alternatively, since a fuzzy controller does not rely on the analysis and synthesis of the mathematical model of the process, the uncertainties of input data from external loads and structural response sensors were treated in a much easier way by the fuzzy controller than with classical control theory. Fuzzy logic uses IF-THEN rules as an interface to connect the inputs and outputs and this means that continuous inputs are transformed into linguistic variables which are then converted into numerical values through defuzzication. In semi-active control, the numerical values provide control commands that vary the mechanical properties of a semi-active control device. In this study, the relative displacement and velocity between the top plate and bottom plate of the MRE TMD were used as inputs to control the lateral stiffness of the MRE TMD controlled by the controller output.

The designing process of a fuzzy controller begins with choosing inputs and outputs, and defining the membership functions. As mentioned before, the inputs chosen were $x_4 - x_3$ and $\dot{x}_4 - \dot{x}_3$. Each input has two linguistic variables which were abbreviated to: P-Positive, N-Negative. The output is the current signal and the linguistic variables were defined as: L-Large, S-Small. Table 3 gives the inference rule based on the two inputs.

Simulation results

A Simulink model that incorporated the three storey building model was built. The swept sinusoidal signal and the scaled 1940 El Centro record (time scale factor is 1:3 and amplitude scale factor is 1:2) were then chosen as the input to the simulation program. The simulation results include the transmissibility responses under the swept sinusoidal signal, and the peak values for the accelerations and relative displacement under El Centro motions, of the third floor and the second floor.

Figure (9) and Figure (10) show the transmissibility responses of the third floor and the second floor-to-ground motion under sweep frequency excitation, respectively. The transmissibility is defined as the ratio of the floor acceleration to the ground acceleration, as shown by Equ. (8). Smaller peak value of the transmissibility means better vibration-reduction performance.

$$T = \frac{\ddot{x}_i}{\ddot{x}_g} \tag{8}$$
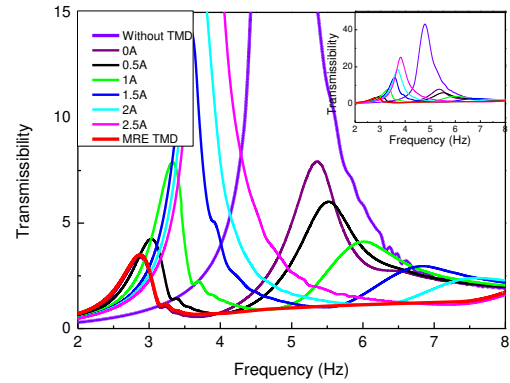
where T is the instant transmissibility.

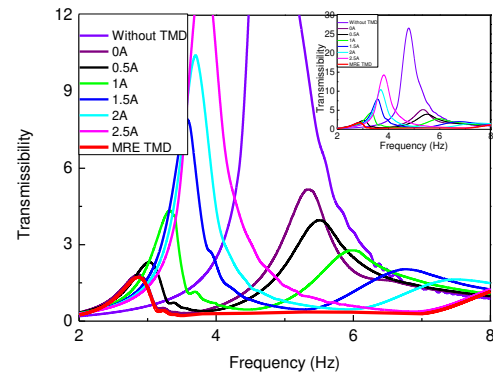
Figure 9. Transmissibility from ground to the third floor.

Figure 10. Transmissibility from ground to the second floor

Table 4. Peak transmissibility with different TMDs (simulation)

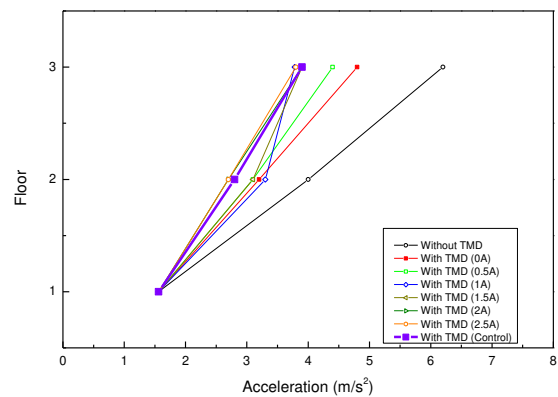| Current (A)	0	0.5	1	1.5	2	2.5	No TMD	Semi-active TMD
	Peak transmissibility							
Second floor	5.3	5.5	4.4	8.1	10.4	14.2	26.7	1.8
Third floor	8.1	6.2	7.8	14.2	18.6	25.4	43.3	3.65

Figure 11. Peak values of acceleration of three floors with respect to the ground.
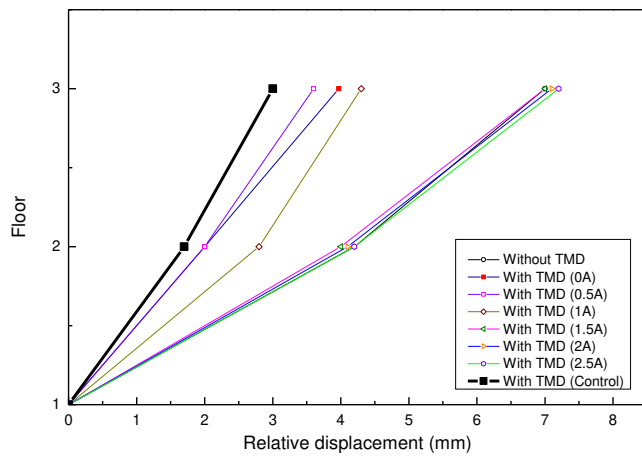
Figure 12. Peak values of relative displacement of three floors with respect to the ground.
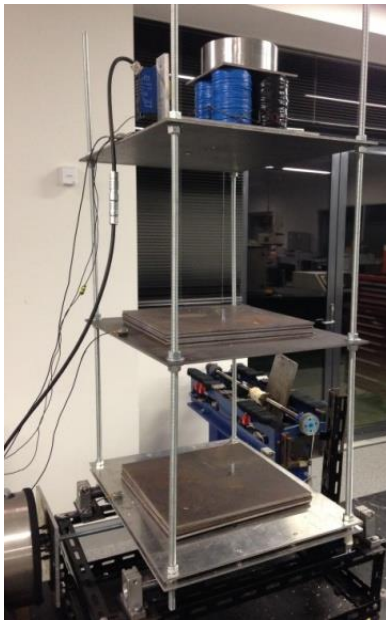

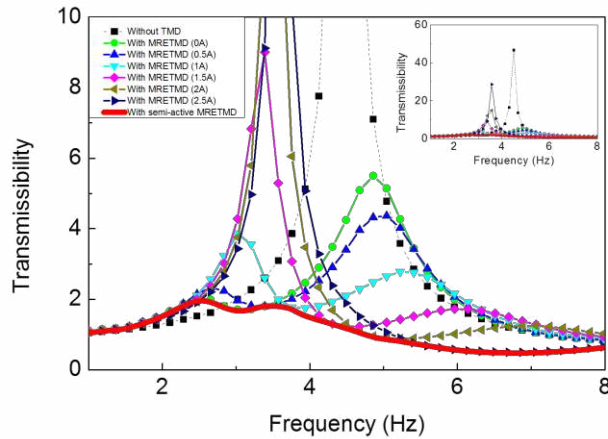Figure 13. Photograph of the practical experimental setup.

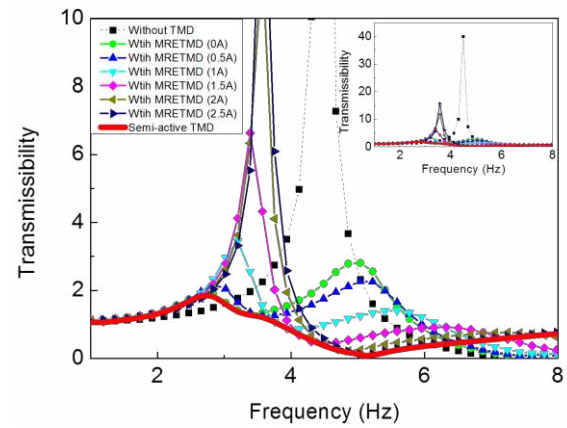Figure 14. Experimentally obtained transmissibility from ground excitation to the third floor.

Figure 15. Experimentally obtained transmissibility from ground excitation to the second floor.

Table 5. Peak transmissibility with different TMDs (experiment)

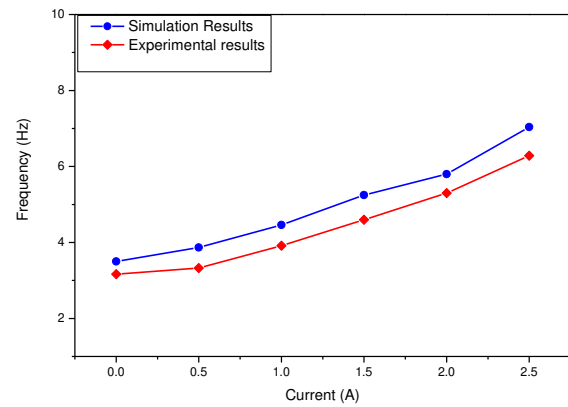| Current (A)	Peak transmissibility							
	0	0.5	1	1.5	2	2.5	No TMD	Semi-active TMD
Second floor	2.9	2.3	3.5	6.6	11.7	15.6	39.8	1.8
Third floor	5.5	4.4	3.8	9.0	14.7	28.6	48.0	2.0

Figure 16. The comparison between the simulation results and the experimental results for the third floor.

For passive TMD, if the natural frequency of the TMD cannot match the earthquake excitation frequency, it will be unable to reduce building vibration and can even make it worse. Because earthquakes are unpredictable and their energy concentration frequency range varies, passive TMD cannot deal with different earthquakes.

Because of this, the passive TMD is not suitable for different earthquakes. In terms of the semi-active TMD proposed in this paper, theoretically if it can reduce the vibration over a wide frequency range, then it can deal with different earthquakes. In order to verify the effectiveness of the MRE TMD over a wide frequency range, sweep

frequency excitation is used to evaluate the performance of the MRE TMD at different frequencies. The simulation results are shown in Figure (9) and Figure (10). Each of the two figures includes eight cases: the building without TMD, six different passive MRE TMDs, and a semi-active TMD. Here the passive TMD means that a constant current was applied to the MRE TMD, such as 0A, 0.5A, etc., so that these passive TMDs are different from each other but with fixed parameters (stiffness and damping). The different passive TMDs are presented as the comparison. The semi-active case means that the parameters of the MRE TMD can be continuously adjusted in real time. From Figure (9) and Figure (10), it can be seen that the test result of the case without TMD has only one peak while the other six passive cases all have two peaks; and that the two peaks of each curve shifted to the right when the current applied was increased. The lowest point between the two peaks of any passive curve indicates the most effective point where the TMD absorbed the largest amount of energy. From Figure 9 and Figure 10, it can be seen that the effective points of each passive MRE TMD are near their natural frequencies and shifted to the right as the current increased. Another important conclusion which can be drawn is that the passive TMD can even make the building vibration worse when its natural frequency does not match the excitation frequency. For example, the passive TMD with constant 1A current increases the transmissibility from 1.6 (without TMD) to 5.8 when the excitation frequency is 3 Hz. In other words, the passive TMD will enhance the building vibration level if the earthquake energy focuses on 3 Hz. In terms of the semi-active MRE TMD, it can vary its natural frequency to trace the excitation frequency based on the short time Fourier transform control algorithm (Sun et al., 2015b). Thus, the semi-active MRE TMD can reach all the most effective points and is shown as the red line in Figure 9 and Figure 10. In other words, the controlled MRE TMD is effective over a large frequency range and thus can deal with different earthquakes. The peak transmissibility of the building with different TMDs is given in Table 4 and the results also verify the semi-active TMD performs the best as the semi-active TMD maintains minimum peak transmissibility.

In order to further verify the effectiveness of MRE TMD, the performance of the MRE TMD controlled by the fuzzy logic control algorithm was evaluated under earthquake excitation. The simulation results are shown in Figure (11) and Figure (12). It can be seen that the peak values of acceleration and relative displacement change as the currents changes, but the semi-active responses remain the best in all cases, especially for relative displacement. These two figures effectively demonstrate that the semi-active MRE TMD outperforms other passive TMDs in terms of reducing the accelerations and relative displacement.

Experimental verification

Experimental setup

Figure 13 shows the whole experimental set-up where the three story building model was fixed onto the platform with the MRE TMD mounted on the top. The first floor stays relatively static with the vibration platform since they are screwed together. Three accelerometers (CA-YD-106) were used to measure the accelerations and displacements of the three floors, respectively. A laser displacement sensor (MICRO-EPSILON Company) was mounted on the top floor to monitor the relative motion between the top plate and the bottom one of the MRE TMD ($x_4 - x_3$). The controller can calculate the other required input signal $\dot{x}_4 - \dot{x}_3$ by doing derivative of the measured signal. The first part of the experiment was conducted by running the whole system under a total of eight swept sinusoidal excitations. The second part used the scaled 1940 El Centro data as the excitation in order to simulate a real seismic scenario. The following subsections present detailed illustrations and analyses.

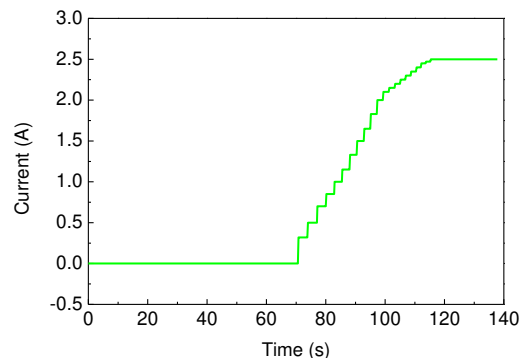### Experimental result under swept excitation

Figure 17 The input current to the MRE TMD under sweep excitation

Figure (14) and Figure (15) show the transmissibility from the ground to the third and the second floors, respectively, under swept sinusoidal excitations. As it is defined in Figures 9 and 10, the transmissibility still indicates the ration of the floor acceleration to the ground acceleration. In this test, a sinusoidal signal with a frequency range sweeping from 1Hz to 10 Hz and amplitude of 10V was used to drive the shaker to excite the horizontal vibration platform. A total of six passive TMDs with different currents and the building without TMD were tested. The observations in the experimentally obtained results match well with those in the simulation results (Figure (9) and Figure (10)). There is only one peak for the case without TMD and two peaks for the six passive cases. The testing results indicate that the most effective vibration absorption points of each passive TMD shifted to the right as the current was increased. The semi-active MRE TMD controlled by a short time Fourier transform control algorithm can trace the excitation frequency and reach the most effective vibration absorption points under each excitation frequency and its transmissibility. The input current for semi-active TMD is shown in Figure 17. The testing results shown in Figure 14 and Figure 15 illustrate that the semi-active TMD outperforms all of the passive TMDs. This conclusion can also be verified by Table. 5. As the response index of the third floor is the most important performance indicators of the effectiveness of the MRE TMD, Figure 16 gives the comparison between the simulation results and the experimental results for the third floor. It can be seen that the two curves progresses consistently with the maximum deviation being 13.6%. This means that the proposed model can predict the performances of the MRE TMD well.

Experiment results under earthquake excitation

Two test cases were included in this section: the one with passive MRE TMDs, and the one with semi-active MRE TMD under fuzzy logic. Figure (18) shows the relative displacement between the ground and the third floor. It can be seen that the building with the passive TMD (no current applied to the MRE TMD) performs worse than the semi-active case where fuzzy logic was used. Similarly, the same observations can be found from Figure (19), which shows the relative displacement between the ground and the second floor.
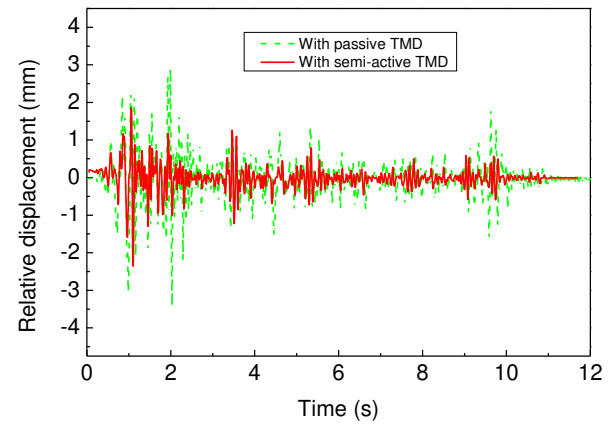

Figure 18. Relative displacement between ground and the third floor.
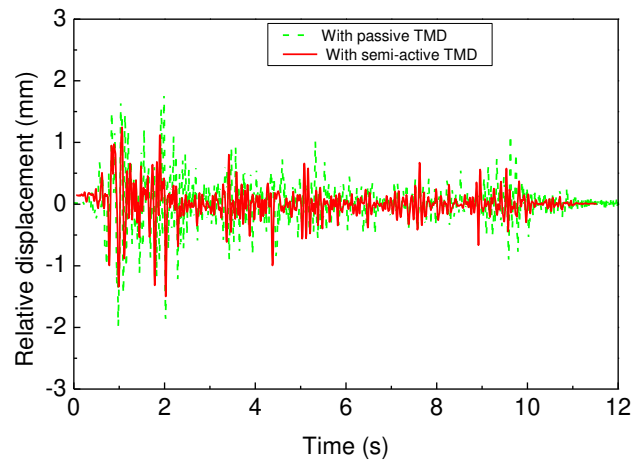

Figure 19. Relative displacement between ground and second floor.

Figure (20) and Figure (21) show the accelerations of the third floor and the second floor in both time domain and frequency domain under two different conditions. It can be seen that the acceleration responses of the semi-active case continually performs better than the passive case. Figure (22) and Figure (23), which corresponds to the simulation results shown by Figure (11) and Figure (12), present the relative acceleration and relative displacement of each floor with respect to the ground, respectively. Similarly, each of the two figures includes eight different tests: the building without TMD, six different passive TMDs, and a semi-active TMD. Each of the six passive cases has fixed parameters but is different from each other due to different current levels, while the semi-active one used fuzzy logic control so that the parameters of the MRE TMD can be continuously adjusted in real time. The peak values of the accelerations and relative displacements under semi-active control remains the smallest of all, especially in terms of

the relative displacement. All of the observations and analyses from the experimental results have shown that this semi-active MRE TMD under fuzzy logic guarantees the best vibration reduction performance among all the tested cases. In order to further detail the performance of TMDs, the RMS of the relative acceleration and relative displacement of each floor with respect to the ground has been given in table 6 and table 7, respectively. The acceleration reduction ratio of the semi-active TMD comparing with the best performed passive TMD is almost zero. However, the relative displacement reduction ratio reaches to 59.6% and 38.9% in terms of the third and second floors, separately. As the relative displacement is a dominant factor on evaluating building damage, it can be concluded that semi-active MRE TMD under fuzzy logic control performs the best on building protection comparing with other passive TMDs.
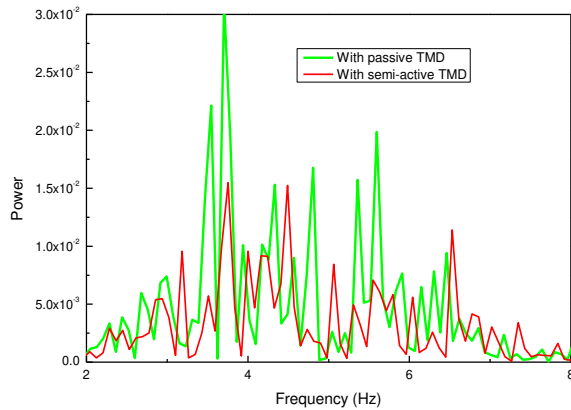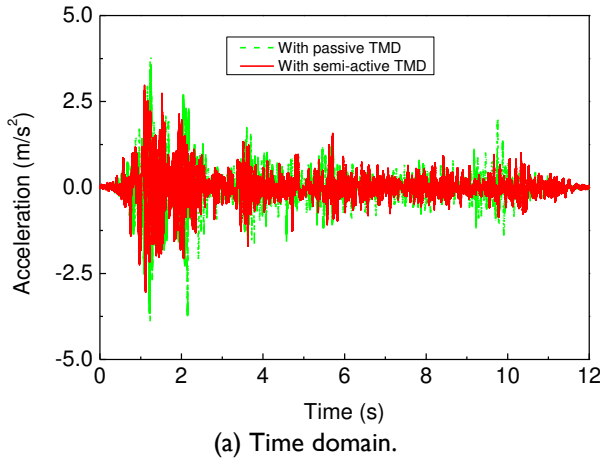

(a) Time domain.

(b) Frequency domain

Figure 20. Acceleration of the third floor

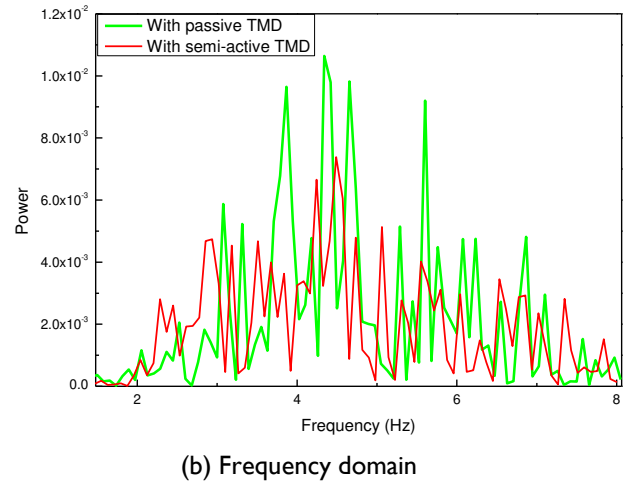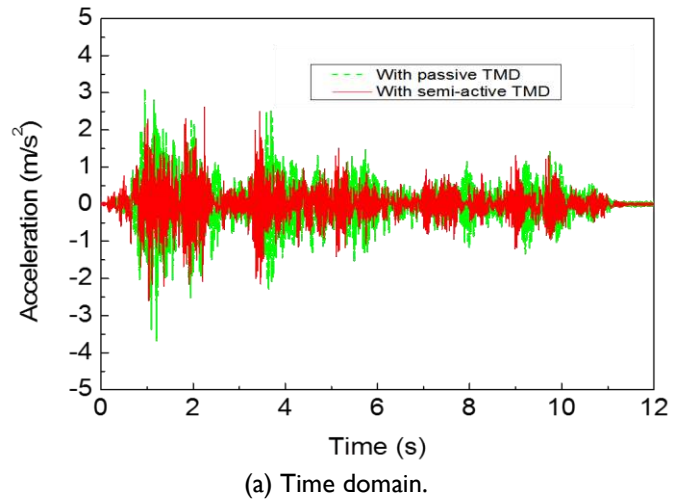(a) Time domain.

(b) Frequency domain
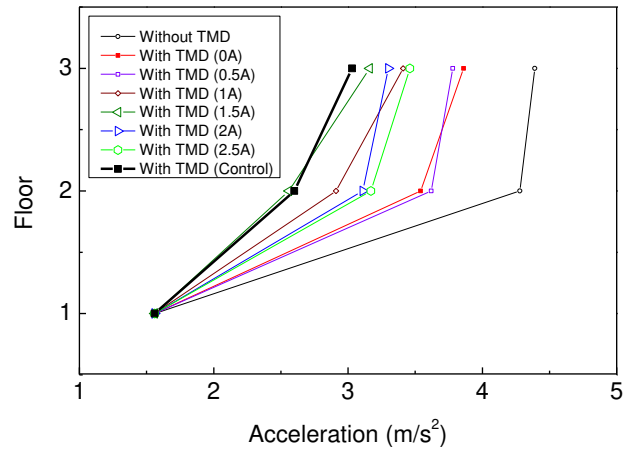
Figure 21. Acceleration of the second floor

. Figure 22. Peak accelerations of the building floors with different TMDs.

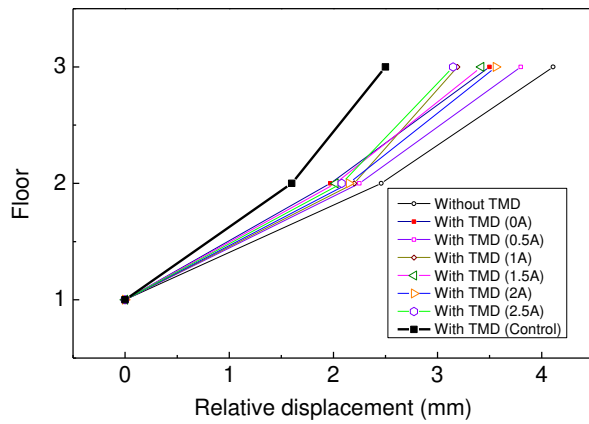Figure 23. Peak relative displacements of the building floors with different TMDs.

This new design not only maintains the advantage of large lateral flexibility but also improves the efficiency of the magnetic field by generating four closed magnetic circuits. The frequency shifted from 3.1Hz to 7.1Hz when the current was changed from 0A to 2.5A and this demonstrated the effectiveness and controllability of the MRE TMD as a method to reduce vibrations. The simulation and experimental results verified the potential of this method to protect the building from ground motion. The transmissibility responses, the relative displacement, and the relative acceleration, as well as the peak displacement and the acceleration have clearly shown the superiority of semi-active MRE TMD over passive TMDs or no TMDs.

Conclusion

This paper introduced an innovative MRE TMD which included four multi-layered MRE structures.

Table. 6. Acceleration RMS of the building floors with different TMDs.

Different TMDs	0A	0.5A	1A	1.5A	2A	2.5A	without	Control	Reduction
Acc of 2nd floor	0.60	0.64	0.51	0.48	0.57	0.52	0.68	0.49	-2%
Acc of 3rd floor	0.57	0.61	0.53	0.50	0.50	0.48	0.72	0.48	0%

Table. 7. Relative displacement RMS of the building floors with different TMDs.

Different TMDs	0A	0.5A	1A	1.5A	2A	2.5A	without	Control	Reduction
x_3-x_1 (mm)	0.59	0.61	0.58	0.57	0.59	0.58	0.69	0.23	59.6%
x_2-x_1 (mm)	0.37	0.40	0.37	0.36	0.38	0.36	0.43	0.22	38.9%

REFERENCES

ALDEMIR, U. 2003. Optimal control of structures with semiactive-tuned mass dampers. *Journal of sound and vibration,* 266, 847-874.

BEHROOZ, M., WANG, X. and GORDANINEJAD, F., 2014. Modeling of a new semi-active/passive magnetorheological elastomer isolator. *Smart Materials and Structures* 23, 045013.

CHANG, J. C. & SOONG, T. T. 1980. Structural control using active tuned mass dampers. *Journal of the Engineering Mechanics Division,* 106, 1091-1098.

DEN HARTOG, J. & ORMONDROYD, J. 1928. The theory of the dynamic vibration absorber. *Transactions of the ASME,* 50, A9-A22.

FISCO, N. & ADELI, H. 2011a. Smart structures: part I—active and semi-active control. *Scientia Iranica,* 18, 275-284.

FISCO, N. & ADELI, H. 2011b. Smart structures: part II—hybrid control systems and control strategies. *Scientia Iranica,* 18, 285-295.

FU, J., LI, P., WANG, Y., LIAO, G. and YU, M. 2016. Model-free fuzzy control of a magnetorheological elastomer vibration isolation system: analysis and experimental evaluation. *Smart Materials and Structures* 25, 035030.

GSELL, D., FELTRIN, G. & MOTAVALLI, M. 2007. Adaptive tuned mass damper based on pre-stressable leaf-springs. *Journal of Intelligent Material Systems and Structures,* 18, 845-851.

HAN, Y., HONG, W. & FAIDLEY, L. E. 2013. Field-stiffening effect of magneto-rheological elastomers. *International Journal of Solids and Structures,* 50, 2281-2288.

JI, H.-R., MOON, Y.-J., KIM, C.-H. & LEE, I.-W. Structural vibration control using semiactive tuned mass damper. The eighteenth KKCNN symposium on civil engineering-KAIST6, Taiwan, 2005. 18-20.

JIANG, G. & HANAGAN, L. M. Semi-active TMD with piezoelectric friction dampers in floor vibration control. Smart Structures and Materials, 2006. International Society for Optics and Photonics, 616915-616915-11.

KANG, J., KIM, H. S. & LEE, D. G. 2011. Mitigation of wind response of a tall building using semi‐active tuned mass dampers. *The Structural Design of Tall and Special Buildings,* 20, 552-565.

KWOK, K. & SAMALI, B. 1995. Performance of tuned mass dampers under wind loads. *Engineering Structures,* 17, 655-667.

LI, Y. & LI, J. 2015. Finite element design and analysis of adaptive base isolator utilizing laminated multiple magnetorheological elastomer layers. *Journal of Intelligent Material Systems and Structures,* 1045389X15580654.

LIAO, G., XU, Y., WEI, F., GE, R. and WAN, Q., 2016. Investigation on the phase-based fuzzy logic controller for magnetorheological elastomer vibration absorber. *Journal of Intelligent Material Systems and Structures*: 1045389X16657417.

LIN, C.-C., LU, L.-Y., LIN, G.-L. & YANG, T.-W. 2010. Vibration control of seismic structures using semi-active friction multiple tuned mass dampers. *Engineering Structures,* 32, 3404-3417.

LIN, P., CHUNG, L. & LOH, C. 2005. Semiactive control of building structures with semiactive tuned mass damper. *Computer‐Aided Civil and Infrastructure Engineering,* 20, 35-51.

MATTA, E. 2011. Performance of tuned mass dampers against near-field earthquakes. *Structural Engineering and Mechanics,* 39, 621-642.

MILLS, R. S. 1979. Model Tests on Earthquake Simulators: Development and implementation of experimental procedures.

NAGARAJAIAH, S. & SONMEZ, E. 2007. Structures with semiactive variable stiffness single/multiple tuned mass dampers. *Journal of Structural Engineering,* 133**,** 67-77.

ORMONDROYD, J. 1928. Theory of the dynamic vibration absorber. *Transaction of the ASME,* 50**,** 9-22.

PADALKA, O., SONG, H., WERELEY, N., FILER, J. & BELL, R. 2010. Stiffness and damping in Fe, Co, and Ni nanowire-based magnetorheological elastomeric composites. *Magnetics, IEEE Transactions on,* 46**,** 2275-2277.

PINKAEW, T. & FUJINO, Y. 2001. Effectiveness of semi-active tuned mass dampers under harmonic excitation. *Engineering Structures,* 23**,** 850-856.

QIN, L., YAN, W. & LI, Y. 2009. Design of frictional pendulum TMD and its wind control effectiveness. *Journal of Earthquake Engineering and Engineering Vibration,* 5**,** 020.

RICCIARDELLI, F., OCCHIUZZI, A. & CLEMENTE, P. 2000. Semi-active tuned mass damper control strategy for wind-excited structures. *Journal of Wind Engineering and Industrial Aerodynamics,* 88**,** 57-74.

SCHRAMM, S., SIHLER, C., SONG-MANGUELLE, J. & ROTONDO, P. 2010. Damping torsional interharmonic effects of large drives. *Power Electronics, IEEE Transactions on,* 25**,** 1090-1098.

SPENCER JR, B. & NAGARAJAIAH, S. 2003. State of the art of structural control. *Journal of structural engineering,* 129**,** 845-856.

SUBRAMANIAM, R. S., REINHORN, A. M., RILEY, M. A. & NAGARAJAIAH, S. 1996. Hybrid control of structures using fuzzy logic. *Computer ‐ Aided Civil and Infrastructure Engineering,* 11**,** 1-17.

SUN, C. & NAGARAJAIAH, S. 2014. Study on semi‐active tuned mass damper with variable damping and stiffness under seismic excitations. *Structural Control and Health Monitoring,* 21**,** 890-906.

SUN, S., CHEN, Y., YANG, J., TIAN, T., DENG, H., LI, W., DU, H. & ALICI, G. 2014. The development of an adaptive tuned magnetorheological elastomer absorber working in squeeze mode. *Smart Materials and Structures,* 23**,** 075009.

SUN, S., DENG, H., YANG, J., LI, W., DU, H. & ALICI, G. 2015a. Performance evaluation and comparison of magnetorheological elastomer absorbers working in shear and squeeze modes. *Journal of Intelligent Material Systems and Structures***,** 1045389X14568819.

SUN, S., DENG, H., YANG, J., LI, W., DU, H., ALICI, G. & NAKANO, M. 2015b. An adaptive tuned vibration absorber based on multilayered MR elastomers. *Smart Materials and Structures,* 24**,** 045045.

WALSH, P. & LAMANCUSA, J. 1992. A variable stiffness vibration absorber for minimization of transient vibrations. *Journal of Sound and Vibration,* 158**,** 195-211.

WEBER, F., BOSTON, C. & MAŚLANKA, M. 2011. An adaptive tuned mass damper based on the emulation of positive and negative stiffness with an MR damper. *Smart Materials and Structures,* 20**,** 015012.

WEBER, F. & MAŚLANKA, M. 2012. Frequency and damping adaptation of a TMD with controlled MR damper. *Smart Materials and Structures,* 21**,** 055011.

XING, Z. W., YU, M., FU, J., WANG, Y., and ZhAO, L. J., 2015. A laminated magnetorheological elastomer bearing prototype for seismic mitigation of bridge superstructures. *Journal of Intelligent Material Systems and Structures:* 26 ,1818-1825.

XU, Z., GONG, X. & CHEN, X. 2011. Development of a mechanical semi-active vibration absorber. *Advances in Vibration Engineering,* 10**,** 229-238.

YANG, J., DU, H., LI, W., LI, Y., LI, J., SUN, S. & DENG, H. 2013. Experimental study and modeling of a novel magnetorheological elastomer isolator. *Smart Materials and Structures,* 22**,** 117001.

YANG, J., SUN, S., DU, H., LI, W., ALICI, G. & DENG, H. 2014. A novel magnetorheological elastomer isolator with negative changing stiffness for vibration reduction. *Smart Materials and Structures,* 23**,** 105023.

ZHOU, L., CHANG, C.-C. & SPENCER, B. 2002. Intelligent technology-based control of motion and vibration using MR dampers. *Earthquake Engineering and Engineering Vibration,* 1**,** 100-110.